Copenhagen '12

X048

Mitigation of Artifacts in RTM with Migration Kernel Decomposition

G. Zhan* (KAUST) & G.T. Schuster (KAUST)

SUMMARY

The migration kernel for reverse-time migration (RTM) can be decomposed into four component kernels using Born scattering and migration theory. Each component kernel has a unique physical interpretation and can be interpreted differently. In this paper, we present a generalized diffraction-stack migration approach for reducing RTM artifacts via decomposition of migration kernel. The decomposition leads to an improved understanding of migration artifacts and, therefore, presents us with opportunities for improving the quality of RTM images.

Introduction

Reverse-time migration (RTM) is a well established imaging method that accurately propagates seismic energy through complex models. The key benefits of RTM compared to other migration methods are that, if the velocity model is accurate enough, it can correctly image any dipping structure, can account for multiple arrivals, and has the capability of providing much higher resolution in the reflectivity image. While enjoying these benefits, RTM is also facing two major problems: high computational costs and strong migration artifacts. With the rapid development of computer hardware in recent years, the former issue may fade away gradually, but the latter one still remains.

Strong amplitude, low-frequency artifacts are often seen on RTM images where a high velocity gradient exists. These artifacts are usually produced by the unwanted cross-correlation of head waves, diving waves and back-scattered waves at the imaging step (Yoon et al., 2004), which severely contaminate the migration image. Various remedies have been proposed to suppress such migration artifacts. For example, a common remedy is to smooth the velocity model before migration to reduce reflections (Loewenthal et al., 1987). Mulder and Plessix (2003) suggested a low-cut filtering on migrated images to reduce migration artifacts. Fletcher et al. (2005) attenuated reflections at boundaries by introducing a directional damping term to the non-reflection wave equation. Guitton et al. (2006) tried to remove the artifacts by using a least-squares filter. Yoon and Marfurt (2006) used the Poynting vector to improve the cross-correlation based imaging condition. Liu et al. (2011) decomposed the full wavefield into their one-way components and applied the imaging condition to the appropriate parts.

In this paper, we decompose the RTM kernel into products of incoming and outgoing Green's functions similar to Liu et al. (2011). Rather than implementing RTM in a conventional way, we adopt a generalized diffraction-stack migration (GDM) algorithm proposed by Schuster (2002), which is equivalent to RTM but with a different implementation. The value of this alternative approach is that it is naturally leads to a filtering of migration operator to reduce RTM artifacts. We now demonstrate its effectiveness for a two-layer model followed by a salt model example. The Green's functions computed from a salt model are decomposed into one-way components, and the cross-correlation imaging condition is applied to appropriate combinations of the wavefield components to produce artifact-free RTM images.

Theory

For a controlled-source seismic experiment, the scattered energy is recorded as data $d(\mathbf{g}|\mathbf{s})$ and, in the frequency domain, the traces can be mathematically approximated as the Born approximation to the Lippmann-Schwinger equation

$$d(\mathbf{g}|\mathbf{s}) \quad = \quad \omega^2 \int_{model\ space} G(\mathbf{x}|\mathbf{s}) m(\mathbf{x}) G(\mathbf{g}|\mathbf{x})\, d\mathbf{x}, \tag{1}$$

where ω is the angular frequency, $G(\mathbf{x}|\mathbf{s})$ is the Green's function for the Helmholtz equation with a background velocity and a point source at $\mathbf{s}$ and trial image point at $\mathbf{x}$. $m(\mathbf{x})$ represents the reflectivity distribution perturbed from the background velocity at $\mathbf{x}$. $G(\mathbf{g}|\mathbf{x})$ is the Green's function with a recording geophone at $\mathbf{g}$ and source at $\mathbf{x}$. Here we have assumed an impulsive source wavelet with amplitude 1.

Migration of seismic data can be carried out by applying the adjoint (Claerbout, 1992) of the forward modeling operator to the data to give the migrated image $m_{mig}(\mathbf{x})$:

$$m_{mig}(\mathbf{x}) \quad = \quad \int_{data\ space} G^*(\mathbf{x}|\mathbf{s}) \ddot{d}(\mathbf{g}|\mathbf{s}) G^*(\mathbf{g}|\mathbf{x})\, dgds, \tag{2}$$

where the $*$ denotes complex conjugation, $\ddot{d}(\mathbf{g}|\mathbf{s}) = \omega^2 d(\mathbf{g}|\mathbf{s})$, and the integration is over the data-space geophone and source variables denoted by $\mathbf{g}$ and $\mathbf{s}$, respectively. Summing equation 2 over all frequencies will give the stacked migration image at the trial image point $\mathbf{x}$.

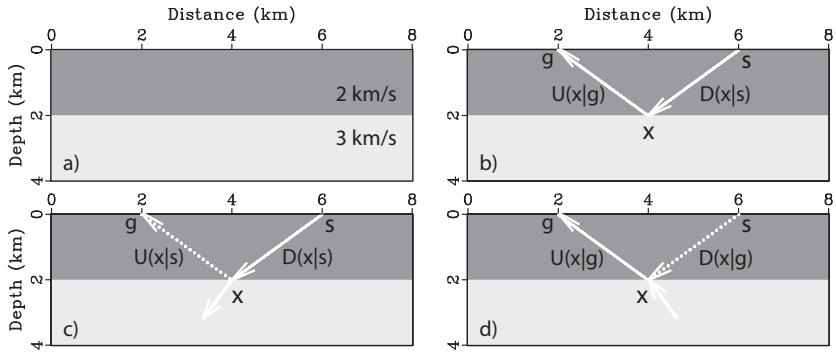

Figure 1 *a) Two-layer model. b) Migration kernel, which is a dot product of the downgoing source and upgoing receiver wavefields. c) Source (running forward) and d) receiver (running backward) wavefields are decomposed into upgoing and downgoing wave components with the ray-diagram interpretation.*

For a two-layer model in Figure 1a with a reflection strength of R, the reflected arrival in the top layer at geophone position $\mathbf{g}$ is given by

$$d(\mathbf{g}|\mathbf{s}) \quad = \quad \frac{R \cdot e^{ik(|\mathbf{s}-\mathbf{x}_{sg}|+|\mathbf{g}-\mathbf{x}_{sg}|)}}{|\mathbf{s}-\mathbf{x}_{sg}| \cdot |\mathbf{g}-\mathbf{x}_{sg}|}, \tag{3}$$

where $\mathbf{x}_{sg}$ is the specular reflection point for source at $\mathbf{s}$ and geophone at $\mathbf{g}$. The Green's function $G(\mathbf{x}|\mathbf{s})$ contains both direct and reflected arrivals in the top layer. Thus, it can be decomposed into two wave components, i.e., a downgoing direct wave $D(\mathbf{x}|\mathbf{s})$ and a upgoing reflected wave $U(\mathbf{x}|\mathbf{s})$

$$G(\mathbf{x}|\mathbf{s}) \; = \; \overbrace{D(\mathbf{x}|\mathbf{s})}^{downgoing-wave} \; + \; \overbrace{U(\mathbf{x}|\mathbf{s})}^{upgoing-wave} \; ; \qquad D(\mathbf{x}|\mathbf{s}) = \frac{e^{ik|\mathbf{s}-\mathbf{x}|}}{|\mathbf{s}-\mathbf{x}|} \;\; and \;\; U(\mathbf{x}|\mathbf{s}) = \frac{R \cdot e^{ik(|\mathbf{s}-\mathbf{x}_{sx}|+|\mathbf{x}-\mathbf{x}_{sx}|)}}{|\mathbf{s}-\mathbf{x}_{sx}| \cdot |\mathbf{x}-\mathbf{x}_{sx}|}, \tag{4}$$

where $\mathbf{x}_{sx}$ is the specular reflection point on the reflector for source at $\mathbf{s}$ and receiver at $\mathbf{x}$ in the top layer. Here the incidence angle dependency in the reflection coefficient R is simply ignored. The same decomposition can be applied to $G(\mathbf{x}|\mathbf{g})$ in a similar way.

Inserting equation 4 into equation 2 gives

$$\begin{aligned} m_{mig}(\mathbf{x}) \quad = \quad \int_{data\ space} [\; & \overbrace{D^*(\mathbf{x}|\mathbf{s})\ddot{d}(\mathbf{g}|\mathbf{s})U^*(\mathbf{x}|\mathbf{g})}^{s_D g_U} \; + \; \overbrace{U^*(\mathbf{x}|\mathbf{s})\ddot{d}(\mathbf{g}|\mathbf{s})D^*(\mathbf{x}|\mathbf{g})}^{s_U g_D} \\ + \quad & \overbrace{U^*(\mathbf{x}|\mathbf{s})\ddot{d}(\mathbf{g}|\mathbf{s})U^*(\mathbf{x}|\mathbf{g})}^{s_U g_U} \; + \; \overbrace{D^*(\mathbf{x}|\mathbf{s})\ddot{d}(\mathbf{g}|\mathbf{s})D^*(\mathbf{x}|\mathbf{g})}^{s_D g_D} \;] \; dgds, \end{aligned} \tag{5}$$

where $\mathbf{x}$ is the trial image point. Each of the terms in the above integrand has a unique physical interpretation and is explained in *Appendix A* of Zhou et al. (1995). The first two terms can be exclusively used to eliminate migration artifacts in RTM, whereas the last two terms can be used to exclusively update the interbed velocity profile. This paper only pursues the elimination of unwanted RTM artifacts.

Examples

For conventional RTM, the first two terms of equation 5 are expected RTM images, whereas the other two are considered as migration artifacts. This is further illustrated in Figure 2. Figure 2a shows the migration image m_{mig} of a single trace with the Figure 1 model and geometry. Figure 2b illustrates the first term in equation 5, and Figures 2c and 2d depict the third and fourth term, respectively. The second term in equation 5 is generated by an upgoing source wavefield striking a horizontal interface from the bottom and reflected downward (Zhou et al., 2005), which does not exist in this example.

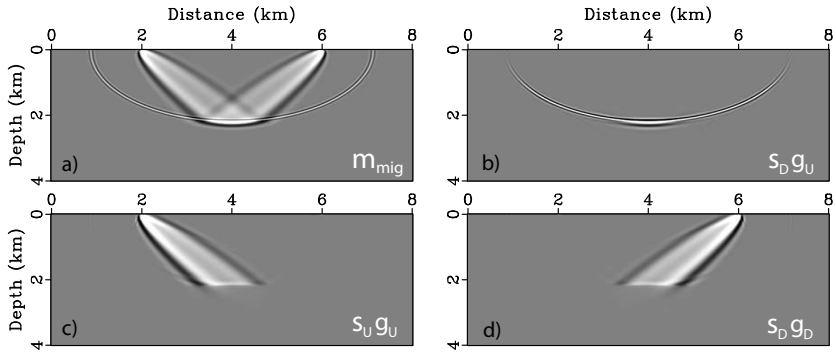

Figure 2 *a) is the migration image of a single trace in a two-layer model. b), c) and d) are the decomposed three image components of a) with equation 5.*

Figure 3 shows another RTM example associated with a salt velocity model. The white polyline shown in Figure 3a demonstrates three different wavepaths that are encountered for this model. Imaging of reflection points at A and C demands the first and second terms of equation 5, respectively. At point B, the incoming and outgoing waves can only be distinguished and decomposed horizontally, i.e., recognized as leftgoing source (s_L) and rightgoing receiver (g_R) wave components. To correctly image point B which resides along the vertical salt flank, the extra $s_L g_R$ term (or $s_R g_L$ term if we exchange the source-receiver location in this case) is needed for equation 5.

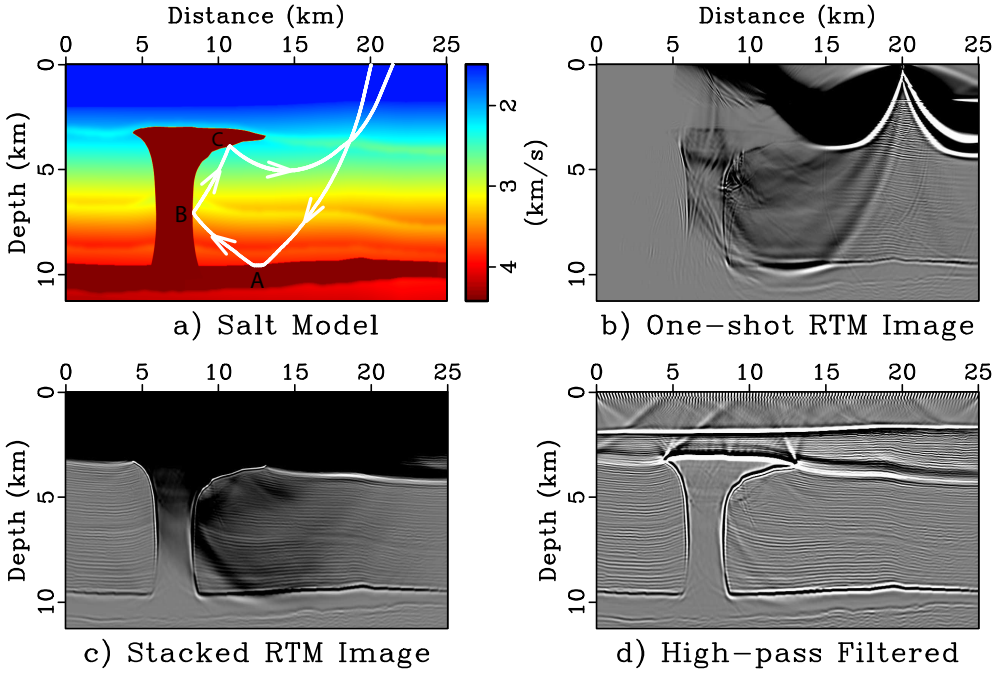

Figure 3 *a) Salt velocity model overlaid by the wavepath of a single source-receiver pair. b), c) and d) are RTM images of this model. Shallow part of the image is overwhelmed by strong artifacts. A high-pass filter is effective to suppress these artifacts but large residuals still remain.*

Figure 4 shows the time evolution of the wavefield which simulates vertical seismic profile (VSP) data (Figure 4b) and reverse vertical seismic profile (RVSP) data (Figure 4c). They can be easily filtered into corresponding one-way components in the F-K domain and then use appropriate parts in equation 5 to get the artifact-free RTM image (Figure 5). The artifacts are successfully eliminated in Figure 5c and the image quality is greatly improved compared to Figure 3d.

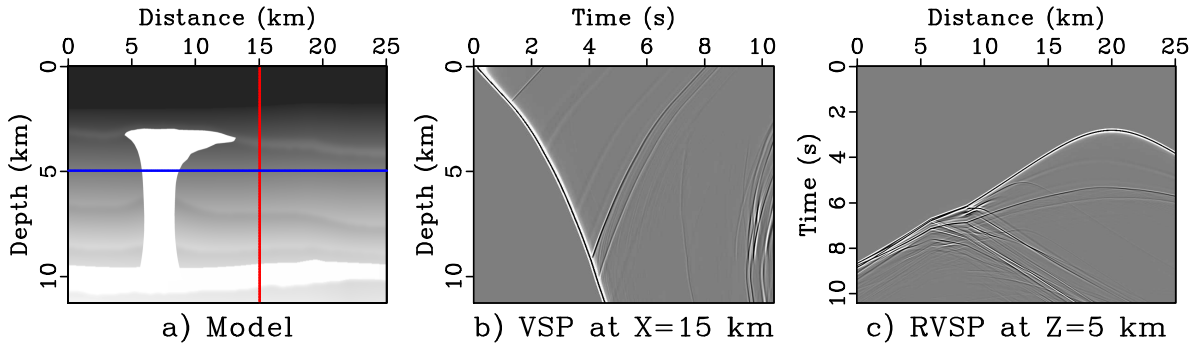

Figure 4 *The Green's functions recorded along the vertical b) and horizontal c) lines.*

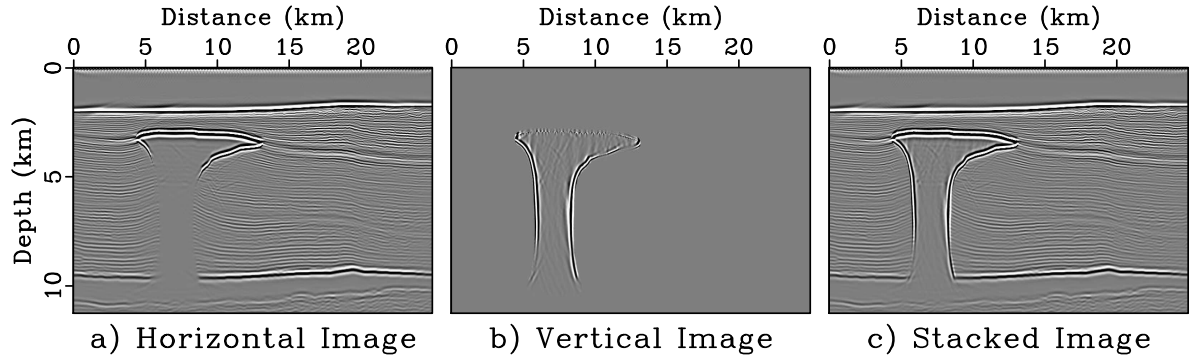

Figure 5 *a) is obtained by cross-correlating downgoing and upgoing wavefield and b) comes from the cross-correlation of leftgoing and rightgoing wavefield. c) is the stack image of a) and b).*

Conclusions

We decomposed the kernel of the RTM imaging operator into products of incoming and outgoing Green's functions. This decomposition not only gives rise to a deeper understanding of the properties of different kernel components but also leads to an imaging algorithm with fewer artifacts and a higher-quality RTM image. The advantage of our approach is that deterministic filtering of the migration kernel can be directly applied to reduce migration artifacts, mitigate multiples and eliminate aliasing artifacts. The drawback is that it requires significantly more storage capacity and I/O time than standard RTM.

References

Claerbout, J. [1992] Earth soundings analysis: processing versus inversion. *Blackwell Science Ltd., London, U.K.*.

Fletcher, R.F., Fowler, P., Kitchenside, P. and Albertin, U. [2005] Suppressing artifacts in prestack reverse-time migration. *SEG Expanded Abstracts*, **24**, 2049–2051.

Guitton, A., Kaelin, B. and Biondi, B. [2006] Least-square attenuation of reverse-time migration artifacts. *SEG Expanded Abstracts*, **25**, 2348–2352.

Liu, F., Zhang, G., Morton, S.A. and Leveille, J.P. [2011] An effective imaging condition for reverse-time migration using wavefield decomposition. *Geophysics*, **76**, S29–S39.

Loewenthal, D., Stoffa, P.L. and Faria, E.L. [1987] Suppressing the unwanted reflections of the full wave equations. *Geophysics*, **52**, 1007–1012.

Mulder, W. and Plessix, R. [2003] One-way and two-way wave-equation migration. *SEG Expanded Abstracts*, **22**, 881–884.

Schuster, G.T. [2002] Reverse-time migration = generalized diffraction stack migration. *SEG Expanded Abstracts*, **21**, 1280–1283.

Yoon, K., Marfurt, K.J. and Starr, W. [2004] Challenges in reverse-time migration. *SEG Expanded Abstracts*, **23**, 1057–1060.

Yoon, K. and Marfurt, K.J. [2006] Reverse-time migration using the Poynting vector. *Exploration Geophysics*, **37**, 102–107.

Zhou, C., Cai, W., Luo, Y., Schuster, G.T. and Hassanzadeh, S. [1995] Acoustic wave-equation traveltime and waveform inversion of crosshole seismic data. *Geophysics*, **60**, 765–773.